

# Screening of effective electrolyte additives for zinc-based redox flow battery systems

David Trudgeon<sup>a</sup>, Kaipei Qiu<sup>a</sup>, Xiaohong Li<sup>a\*</sup>, Tapas Mallick<sup>a</sup>, Oluwadamilola O. Taiwo<sup>b</sup>, Barun Chakrabarti<sup>b</sup>, Vladimir Yufit<sup>b</sup>, Nigel Brandon<sup>b</sup>, David Crevillen-Garcia<sup>c</sup>, Akeel Shah<sup>c</sup>

<sup>a</sup> *Renewable Energy Group, College of Engineering, Mathematics and Physical Sciences, University of Exeter, Penryn Campus, Cornwall TR10 9FE, UK*

<sup>b</sup> *Department of Earth Science & Engineering, Imperial College London SW7 2AZ, UK*

<sup>c</sup> *School of Engineering, University of Warwick, Coventry, CV4 7AL, UK*

## Abstract

The purpose of this work is to assess the suitability of potential electrolyte additives for zinc morphology control and improved electrochemical performance of the zinc electrode for application in zinc based redox flow battery (RFB) systems. Based on existing literature in the field, sixteen candidates are selected, including four metallic additives, two non-ionic surfactants and ten quaternary ammonium compounds. The electrochemical performance of the zinc electrode is assessed using cyclic voltammetry, linear sweep voltammetry and zinc half-cell cycling tests using chronopotentiometry. Zinc electrodepositions are carried out using chronopotentiometry in order to assess the effect of additives on zinc morphology with scanning electron microscopy. Based on zinc reduction and oxidation reaction potentials, the cycling efficiencies, and the effect on zinc morphology, the most promising additives of those tested are tetraethylammonium hydroxide and tetraethylammonium bromide. Both provide smooth and compact zinc deposits and zinc electrode coulombic efficiencies of 95-97 %

---

\* Corresponding author. *Email:* X.Li@exeter.ac.uk Tel: 0044 (0)1326 255769

without leading to significant changes in the zinc reduction/oxidation overpotentials, yielding anodic and cathodic current densities of 77-78 mA cm<sup>-2</sup> and 31-32 mA cm<sup>-2</sup> at overpotentials of +/- 50 mV, respectively. In a zinc-nickel flow cell, these additives provide energy efficiencies of 78-79 %, compared with 69 % without an additive.

**Keywords:** Electrolyte additive; Zinc electrode; Zinc electrodeposition; Redox flow battery

## 1. Introduction

The research and development of zinc based redox flow batteries (Zn-RFBs) commenced in the mid-1970s with the zinc-chlorine and zinc-bromine systems. Featuring fast kinetics, relatively high energy density, and the utilisation of inexpensive materials, Zn-RFB technologies have attracted renewed attention from both academia and industry over the last two decades. Several versions of Zn-RFBs, such as zinc-ferricyanide, zinc-bromine, zinc-nickel, zinc-cerium, zinc-air and zinc-polymer show promise for peak shaving and load levelling applications [1-8]. While the acidic zinc-bromine system is being commercialized by several companies, the only alkaline based zinc system currently available is the zinc-ferricyanide by ViZn Inc. [8]. However, major challenges such as the formation of zinc dendrites, electrode shape change, and hydrogen evolution during charge affect the zinc electrode. To avoid zinc dendrite formation, zinc electrodeposition and dissolution must be better controlled. Electrolyte additives are a promising solution to these challenges, with suitable additives enabling a compact and uniform zinc electrodeposition, improving the cycle life of the battery by allowing more complete dissolution of the zinc deposition on each cycle, thus depressing the build-up of materials on the electrode and maintaining the Zn(II) concentration at a stable level. As a consequence, the battery performance is improved and battery life extended [9,10]. For zinc systems in acidic media, previous work demonstrates compact and dendrite free zinc electrodepositions in methanesulfonic acid with or without the addition of electrolyte additives [11]. However, producing such zinc morphologies is more challenging from alkaline electrolytes.

Heavy metals have traditionally been utilised as additives, including mercury, cadmium, lead or its oxides which can be either alloyed into the zinc electrode during manufacture or added to the electrolyte in the form of soluble salts [12,13]. These heavy metals have high hydrogen overpotentials, so are effective inhibitors for hydrogen evolution

and possess reduction potentials close to that of zinc, enabling co-deposition along with zinc during the charge phase. The additives block the active deposition sites, thus suppressing both dendritic zinc morphology and the corrosion of zinc. However, environmental concerns make the use of such metals undesirable.

As an alternative, oxides and hydroxides of iron, bismuth, calcium, magnesium, indium, tin and tungsten [14-20] in addition to fluorides, phosphates and borates [21] have been investigated. For example, Wen et al. demonstrated that the addition of tungstate to the electrolyte could produce a smooth and compact zinc morphology and high coulombic efficiencies in excess of 90 % [14]. However, a high concentration of sodium tungstate (0.6 M Na<sub>2</sub>WO<sub>4</sub>) is required in order to achieve these effects. Previous work by Justinijanovic et al. and Yuan et al. shows that tin ions can modify zinc morphology in concentrations of as low as 1 mM, with much improved morphology obtained at concentrations of 1.44 mM [15,16]. The same works demonstrate a coulombic efficiency of the zinc electrode of 95 % or more in the presence of tin chloride additive, as well as significant suppression of the zinc corrosion reaction and the associated electrode shape change. Thornton and Carlson [21] report properties of electrolytes containing high concentrations of fluoride, phosphate and borate ions, and find that the solubility of ZnO and the availability of hydroxyl ions in such electrolytes is reduced. As such, they conclude that these compositions should suppress zinc dendrite formation and electrode shape change. However, the use of such high concentrations of additives also reduces the utilisation of active material, thus compromising electrochemical performance. Bismuth has previously been studied as an addition to the electrolyte by Wang et al. [20] who find that a 0.16 g L<sup>-1</sup> concentration of Bi<sup>3+</sup> ions effectively suppresses zinc dendrite formation. McBreen and Gannon [18] have shown that additions of 2 to 10 % wt. of Bi<sub>2</sub>O<sub>3</sub> to the electrode could prevent dendritic zinc morphologies.

Organic additives receive considerable attention and the common additives include poly (vinyl alcohol), polyethylene glycol (PEG), polyethylenimine (PEI), quaternary ammonium salts, polytetrafluoroethylene (PTFE), and cellulose [22-33]. It is generally agreed that the organic additives are specifically adsorbed at rapid growth sites (i.e. dendrites) on the surface of the electrode and restrict further growth at these locations. Thus, the presence of organic additives promotes uniform zinc deposition by refining the grain size and eliminating dendritic growth. Diggle and Damjanovic [23] report that tetrabutylammonium ions are effective additives in alkaline zincate solutions and suppress the growth of dendrites, leading to more compact zinc deposits. However, excessive concentrations can lead to inhibition of zinc deposition and a decrease in charge efficiency. Several organic surfactant additives are studied by Zhu et al. [24], including three perfluorosurfactant variants and the quaternary amine surfactant cetrimonium bromide (CTAB). This work shows that at low concentrations of 30-60 ppm these additives can significantly suppress hydrogen evolution and improve zinc deposition morphology. Lan et al. [26] study several quaternary ammonium hydroxides as additives and find that all can modify zinc morphology and improve coulombic efficiency to some extent. In addition, various polyamines and combinations of these are studied [28] resulting in improved zinc morphology. Further work on non-ionic organic additives includes polyethylene glycol and polyethylenimine [29-32], with work by Banik and Akolkar showing that both polyethylene glycol (M.W. = 200 g mol<sup>-1</sup>) [29] and polyethylenimine (M.W. = 800 g mol<sup>-1</sup>) [32] can be effective suppressors of zinc dendrite formation.

Although numerous potential additives are identified in the previous work discussed above, only a few candidates have been studied simultaneously, and the work of different researchers is carried out under different experimental conditions, making direct comparison difficult. Therefore, this work selects the most promising additives from those previously

considered and compares them under identical experimental conditions, including preliminary evaluation of those selected in a zinc-nickel flow cell. The aim is to identify and quantify the effect of the most promising additives for use in zinc based alkaline flow battery systems. The effects of additives on electrochemical performance are assessed through cyclic voltammetry, linear sweep voltammetry and zinc deposition/dissolution cycling. The morphology of zinc deposits is analysed through scanning electron microscopy, and the performance of the most promising additives is investigated in a zinc-nickel redox flow cell.

## **2. Experimental**

### ***2.1. Electrolyte Chemicals***

The base electrolyte in use is a 6 M KOH (Acros Organics, analytical grade, 85 %) and 0.5 M ZnO (Fisher Chemical, AR grade, 99.5+ %) solution, unless otherwise stated. A complete list of the additives tested is shown in **Table 1**. All chemicals are used as received.

### ***2.2. Electrode materials and preparation***

The zinc electrode substrate employed for cyclic voltammetry, half cell and full flow cell cycling tests is prepared using a graphite polymer composite (Eisenhuth, BMA5 graphite/polyvinylidene fluoride). For linear sweep voltammetry a zinc foil is used as the working electrode substrate (Goodfellow, 1 mm thickness, 99.95 % purity). All electrodes are prepared by first cutting into segments of 1.5 cm × 5 cm. These are then polished using emery paper (Simply Brands, Wet and Dry Paper, 3000 grit) washed with deionised water, then masked to expose an area of 0.25 cm<sup>2</sup> (0.5 cm × 0.5 cm) using polypropylene tape with an acrylic adhesive (Avon tapes, AVN9811060K, 25 µm thickness) before a final rinse with deionised water prior to use. The Hg/HgO reference electrode is prepared in a 6 M KOH solution using the following chemicals; mercury (Acros Organics, 99.999 % metals basis), mercury (II) oxide (Acros Organics, 99+ %). The counter electrode is a platinum mesh (Alfa

Aesar, 99.9 % metals basis, 0.1 mm dia. wire, 52 mesh). For zinc-nickel flow cell tests, the zinc electrode substrate is a graphite polymer, cut into 2 cm × 2 cm pieces and polished with emery paper. The nickel electrode is a sintered nickel, cut into 2 cm × 2 cm pieces.

### **2.3. Electrochemical methods**

All electrochemical measurements are taken using a BioLogic SP-300 potentiostat and EC-Lab software. Cyclic voltammetry, linear sweep voltammetry, chronopotentiometry and zinc half-cell cycling tests are carried out in a 20 ml glass cell using a three-electrode half-cell configuration. For this, an Hg/HgO reference electrode in 6 M KOH is employed with a platinum mesh counter electrode and either a graphite polymer or zinc foil working electrode, using the materials and preparation method described previously. Cyclic voltammetry is carried out at 20 mV s<sup>-1</sup> between -0.5 and -1.6 V vs Hg/HgO on a graphite polymer substrate, and linear sweep voltammetry at 10 mV s<sup>-1</sup> between -1.26 and -1.46 V vs Hg/HgO on zinc foil.

Zinc deposits are obtained with and without the additives on a graphite polymer substrate using chronopotentiometry at 20 mA cm<sup>-2</sup> for 1 h in order to allow the effect of additives on zinc morphology to be assessed by SEM. Half-cell cycling tests are carried out over 11 cycles using chronopotentiometry at 100 mA cm<sup>-2</sup> for 12 minutes to investigate the change in coulombic efficiency caused by the additives. For this, the electrolyte is stirred throughout at 1500 rpm using a Camlab MS-H280-Pro magnetic stirrer and a PTFE stir bar in order to minimise diffusion limitations.

Full zinc-nickel flow cell cycling tests are conducted using a C-Flow laboratory cell (C-Tech Innovation, 1 cm × 1 cm working electrode area, 1.2 cm electrode gap). The positive electrode is a commercial sintered nickel plate (Jiansu Highstar Battery Manufacturing Co. Ltd.). The negative electrode is a graphite/polyvinylidene fluoride composite. A peristaltic

pump (Watson-Marlow 323S) and Marprene tubing (Watson Marlow, 3.2 mm I.D., 6.4 mm O.D.) are employed to pump 250 ml of the electrolyte solution containing 6 M KOH + 0.5 M ZnO + 5 mM additive throughout the test at a volumetric flow rate of 700 ml min<sup>-1</sup>, providing an average linear velocity of 9.7 cm s<sup>-1</sup>. All of the electrochemical measurements are carried out at room temperature (293 K). The surface morphology of the samples is characterised using a Hitachi S-3200N SEM, operated at an accelerating voltage of 20 kV and a working distance of 15 mm.

### 3. Results and discussion

#### 3.1. Deposition and dissolution of zinc

**Fig. 1** reports a typical cyclic voltammogram for zinc deposition and dissolution at a polished graphite polymer substrate. On the negative scan, the onset of zinc reduction occurs at -1.45 V vs. Hg/HgO with cathodic current density rising sharply to a reduction peak at -1.5 V. A second increase in cathodic current is observed from -1.8 V, associated to hydrogen evolution. On the positive scan, reduction continues to -1.42 V vs. Hg/HgO and the current immediately becomes anodic with a well-formed and symmetrical anodic peak at -1.32 V. The nucleation loop observed between -1.45 and -1.42 V vs Hg/HgO is a classical response for the deposition and dissolution of a metal onto a foreign substrate where nucleation and growth of the new phase is required. The ratio of the charges for zinc dissolution and deposition,  $Q_{\text{anodic}}/Q_{\text{cathodic}}$ , is 0.76. It is apparent that the kinetics of the Zn<sup>2+</sup>/Zn redox couple are moderately fast, and that substantial overpotentials are associated with the nucleation of zinc onto the graphite polymer electrode substrate. The low charge efficiency is caused by incomplete oxidation of the deposited zinc and the competing hydrogen evolution reaction during zinc deposition. Indeed, at more negative potentials a second increase in cathodic current can be seen at -1.8 V vs. Hg/HgO and some hydrogen bubbles are observed if the potential is held at -1.8 V and below.

As illustrated in **Fig. 2**, cyclic voltammetry is carried out in order to assess the effect of each additive on the zinc deposition and dissolution reactions. The corresponding charge efficiencies are presented in **Table 2**. In general, all of the additives have positive effect on charge efficiency. The greatest increases, yielding efficiencies of 91-95% (compared with 76% with no additive), are obtained in the presence of the tetrapropylammonium and tetrabutylammonium bromides and hydroxides. For the metallic additives, as shown in **Fig. 2a**, there is no significant change in cyclic voltammetric performance when compared to the no additive case. This could be a result of the low proportion of addition (1 mM in this experiment). On the other hand, experimental work carried out by Yuan et al. [16] demonstrates, with higher concentration of  $\text{Sn}^{2+}$  ions of  $5.6 \text{ g L}^{-1}$ , clear additional peaks for both reduction and oxidation of tin. In previous research work [18, 19] it is observed that, if the reduction potential of the metal is too positive compared to zinc, the secondary metal will be co-deposited with zinc but is unlikely to be oxidised within the operational potential range of the cell. Thus, with continued cycling, the added metal will form a permanent layer on the electrode, and zinc deposition will take place onto this layer. This is known as substrate effect [13, 26]. Iron and tin additives may therefore be considered to be more suitable for incorporation into the zinc electrode substrate, rather than adding them into the electrolyte.

Cyclic voltammograms for the non-ionic surfactants are shown in **Fig. 2b**, which demonstrate that PEI 800 causes a significant increase in the zinc reaction overpotentials. As seen from the voltammograms, zinc reduction commences at  $-1.52 \text{ V}$  vs. Hg/HgO and oxidation starts at  $-1.35 \text{ V}$  compared with  $-1.42 \text{ V}$  and  $-1.37 \text{ V}$  in the case of no additive. The anodic/cathodic peak separation ( $\Delta E_p$ ) is clearly also increased, being  $384 \text{ mV}$  in the presence of PEI 800 compared with  $220 \text{ mV}$  with no additive. This is due to the potential driven adsorption of the additive onto preferred zinc deposition locations on the electrode which causes a blocking effect, suppressing zinc reduction and, to a lesser extent, zinc oxidation, this

observation is in agreement with previous work on this additive [32]. The effect of PEG 200 on overpotentials and peak separation is relatively insignificant. It is thought that the larger effect of PEI 800 is due predominantly to its larger molecular structure compared with PEG 200, which increases the blocking effect and required overpotentials.

**Fig. 2c** and **Fig. 2d** represent the results of cyclic voltammetry for the additive groups of quaternary ammonium bromides and hydroxides, respectively. For zinc reduction, the methyl and ethyl group additives have little effect. In the presence of hexadecyl trimethyl additives, the onset of zinc reduction occurs at -1.45 V vs. Hg/HgO. For the propyl group additives, reduction commences at -1.48 V vs. Hg/HgO. The butyl additive group shows unusually large overpotentials in comparison to the other additive groups studied, with reduction not occurring until the potential reaches -1.68 V vs. Hg/HgO. For zinc oxidation, the effect of additives is relatively insignificant in all cases except with butyl additives, for which oxidation commences at -1.32 V.

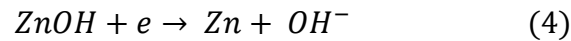
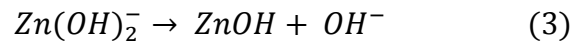
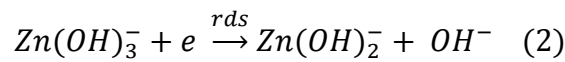
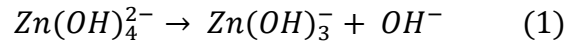
As shown in **Table 2**, the anodic/cathodic peak separation is increased by around 50 mV with CTAB and HDTMAH, by 85-89 mV with TPAB and TPAH additives and by around 230 mV with TBAB and TBAH. There is a clear trend in the increase in overpotentials relating to the size of the alkyl chains. Larger ammonium group additives cause increased overpotentials for zinc reduction, with the order of the alkyl chains in terms of small to large overpotential being; methyls → ethyls → hexadecyl trimethyls → propyls → butyls, regardless of whether the anion is hydroxide or bromide. This can be explained by the fact that the inhibition effect of quaternary ammonium additives relates to the length of the alkyl chains which decrease the polarity of the additive due to their ability to repel electron density toward the nitrogen atom (i.e. in the ammonium cation). In addition, this has the effect of increasing hydrophobicity with increasing alkyl chain lengths. This finding is in

good agreement with previous studies of quaternary ammonium additives and is supported by previous research [25, 26]

Linear sweep voltammetry is carried out in order to support the results of cyclic voltammetry. In this case, tests are carried out over a small potential range, defined as +/- 100mV versus the crossover potential, -1.36 V vs Hg/HgO. In order to remove the influence of zinc nucleation on the graphite substrate and to simulate the operation of the zinc electrode in a real battery system, in which zinc deposition will occur onto pre-existing zinc after the first few cycles, a zinc foil electrode substrate is employed. The anodic and cathodic current densities at +/- 50 mV vs. crossover potential are provided in **Table 2**, giving quantitative data on the suppression of zinc reduction and oxidation by the additives. The linear sweep voltammograms themselves being included in the supplementary data. This confirms the results of the cyclic voltammetry discussed previously, showing that the metallic additives, methyl and ethyl quaternary ammonium additives and PEG 200 have relatively little effect on the current densities. Cathodic current densities at  $\eta = -50\text{mV}$  are reduced by around 59 % with CTAB and HDTMAH, 75 % with TPAB and TPAH, 85 % with PEI 800 and 88 % in the presence of TBAB and TBAH. Anodic current densities at  $\eta = 50\text{mV}$  are reduced by 44-47 % with CTAB and HDTMAH, 85 % with TPAB and TPAH, 91 % with PEI 800 and 92 % in the presence of TBAB and TBAH.

While the results of cyclic voltammetry demonstrate that most of the additives have the potential to improve the coulombic efficiency of zinc reduction/oxidation, the increased anodic/cathodic peak separation and reduced current densities at  $\eta = +/- 50 \text{ mV}$  show that many of the additives cause significant suppression of the zinc reduction and oxidation reactions, which will inevitably reduce the voltaic efficiency of a full cell or battery system. Taking this into consideration, the most promising additives at this stage are the tetramethyl and tetraethyl ammonium additives and PEG 200.

A mechanism of zinc deposition and dissolution is proposed by Bockris et al. [34] as shown below. This four-step mechanism is written in the cathodic direction, the anodic reaction proceeds through the exact reverse of the above path, in which, the steps (2) and (4) incorporate a single electron charge transfer, and step (2) is also the rate-determining step (rds).



It is generally accepted that by adsorption of quaternary ammonium additives to the preferred zinc reduction sites (i.e., dendrite propagation locations) the rate of reactions (2) and (4) are suppressed, requiring larger overpotentials to take place. Thus, the greater blocking effect of the quaternary ammonium additives with longer alkyl chains causes increased overpotentials for the zinc reduction and oxidation reactions, predominantly due to the suppression of the reduction reaction (2), which is the rds but also the reduction reaction (4), as zinc is forced to electrodeposit at less preferred locations. This blocking effect of non-ionic and quaternary ammonium additives has the positive effect of providing smoother and more compact zinc electrodepositions, but also the negative effect of increasing zinc deposition and dissolution overpotentials, thus reducing voltaic efficiencies.

### **3.2. SEM characterisation of zinc electrodepositions**

SEM is conducted on zinc deposits obtained from 6 M KOH/0.5 M ZnO base electrolytes with 1 mM concentrations of metallic additives and 5 mM concentrations of organic additives. The depositions are carried out at 20 mA cm<sup>-2</sup> for 1 h in a static electrolyte.

**Fig. 3** shows SEM images of the deposits obtained with no additive and in the presence of metallic additives. With no additive (**Fig. 3a**), the morphology is clearly mossy and porous. With the metallic additives, the deposit in the presence of Bi<sub>2</sub>O<sub>3</sub> additive (**Fig. 3b**) is largely smooth, with some small boulder-like protrusions. With SnCl<sub>2</sub> additive (**Fig. 3c**) the deposit has a smoother and more consistent morphology. With FeBr<sub>2</sub> (**Fig. 3e**) the morphology shows some improvement compared to the case of no additive, but the deposit consists of boulder-like structures and is not as smooth or compact as with SnCl<sub>2</sub> or Bi<sub>2</sub>O<sub>3</sub>. With SnO additive (**Fig. 3d**) the morphology shows only a slight change in comparison to that of no additive. For the non-ionic surfactants (**Fig. 3**), the deposits are largely compact, but some boulder-type structures remain, especially in the case of PEI 800.

**Fig. 4** and **Fig. 5** show that for TEAB and TEAH the morphology is more consistent and consists primarily of granular components around 2 μm in length. This supports the observation from the work of Diggle and Damjanovic [23]. TPAH and TBAH cause a mixed morphology with mostly mossy deposits consisting of needle-like components, together with some more crystalline elements. The CTAB deposit appears broadly similar to that seen with TPAB, which consists mainly of hexagonal platelets around 0.5 μm in diameter, rather than needle-like structures. HDTMAH leads to a more compact and crystalline deposit, consisting of the same hexagonal platelets observed with TPAB. Interestingly, TBAB shows a significantly modified morphology, consisting of long fibrous elements up to 5 μm in length.

### **3.3. Half-cell cycling of zinc electrode**

For each of the 16 additives, coulombic efficiencies at half-cell cycling of a zinc electrode are averaged over eleven cycles for each additive and the results shown in **Table 2**. It can be seen that seven organic additives including PEI 800, PEG 200, TEAB, TPAB, CTAB, TEAH, and HDTMAH have improved coulombic efficiencies in the range of 93-97% compared to that of 87% with no additive. **Fig. 6** shows an example result from the zinc half-

cell cycling tests with additive of TEAH which gives an average coulombic efficiency of 97%. On the other hand, with TBAB and TBAH, coulombic efficiencies are decreased to 74 % and 32 %, respectively. For these two additives, localised needle-like dendrites are observed forming on the electrode during zinc deposition, many of which detach at the beginning of the dissolution phase, thus reducing the zinc available for dissolution and consequently reducing the coulombic efficiency. This behaviour can be explained by the relatively large size of the butyl group, which causes increased inhibition effects on parts of the electrode surface due to higher steric hindrance [26]. The current density at the remaining exposed sites is therefore increased significantly, causing the formation of localised dendrites. From the zinc half-cell coulombic efficiencies, the butyl ammonium additives obviously possess too strong a polarity to achieve uniform coverage, this also evidenced from cyclic voltammetry measurements as discussed in section 3.1.

For the quaternary ammonium additives, the ethyl and propyl groups (TEAB, TEAH, TPAB, TPAH) demonstrate the highest coulombic efficiencies, at 94-97 %, followed by TMAB and TMAH with 88% and 89 % respectively. The butyl group additives (TBAB and TBAH) however show reduced coulombic efficiencies as discussed above. Both PEI 800 and PEG 200 exhibit improvements in coulombic efficiency at 94% and 95 % respectively while for the metallic additives, only Bi<sub>2</sub>O<sub>3</sub> shows significantly improved coulombic efficiency of 92%. According to McBreen and Gannon [18], bismuth is not removed from the electrode during electrode discharge. During charge, the additive will therefore be progressively deposited on to the electrode prior to zinc, due to its more positive standard potential compared to zinc, removed from the electrolyte over a large number of cycles forming a bismuth substrate onto which zinc is deposited. As such, the positive effect of this additive may be due to the substrate effect, which modifies the polarizability and current distribution of the electrode [18-21], rather than a co-deposition mechanism. In addition, the larger

hydrogen overpotential of bismuth compared to zinc may suppress hydrogen evolution, resulting in improved coulombic efficiency. The absence of secondary anodic and cathodic peaks the presence of the other metallic additives tested in **Fig. 2a** suggests that this is also the case for iron and tin additives. Therefore, these additives may be suitable for incorporation into the zinc electrode substrate, as studied in previous works [16-17], but offer no additional benefit as an additive to the electrolyte.

Despite the fact that most additives show comparable or improved coulombic efficiencies, the suppression of the zinc reduction and oxidation reactions associated with some of these is likely to negate the improved coulombic efficiencies in a full cell system by decreasing the full cell voltaic and energy efficiencies. Therefore, the most promising additives are those that provide improved coulombic efficiencies and smooth and compact morphologies, without significant modification of the reduction and oxidation potentials. From the data in **Table 2** and SEM characterisation, the most promising additives are identified as PEG 200, TEAH, and TEAB.

#### ***3.4. Zinc-nickel flow cell cycling of selected additives***

Based on the experimental data in the previous section, TEAB, TEAH, and PEG200 are selected, their cycling performance is tested in a full zinc-nickel flow cell and the effects on the system efficiency are compared to that of no additive. The zinc-nickel system has a cell potential of 1.73 V, consisting of the two electrode reactions (5) and (6). The flow cell used in this work employs a graphite/polyvinylidene fluoride negative electrode, a sintered nickel positive electrode, an inter-electrode gap of 1.2 cm and a 6 M KOH + 0.5 M ZnO electrolyte solution with 5 mM of the additives. It is cycled by charging with a current density of 20 mA cm<sup>-2</sup> for 15 min followed by discharge at the same current density until the cell voltage drops to 0.8 V.



**Fig. 7** reports the energy efficiencies during the 50 charge/discharge cycle experiments with and without additives. The coulombic, voltaic and energy efficiencies are averaged over the 50 cycles and the results are shown in **Table 3**. From the table, it can be seen clearly that TEAH and TEAB provide impressive increase in coulombic efficiency at 90% and 89%, respectively, compared to 77 % with no additive. The energy efficiencies are accordingly improved with these additives, reaching 79% and 77 % respectively compared to 69 % with no additive. This supports the results obtained from the zinc half-cell cycling that show coulombic efficiencies of up to 97 % compared with 87 % with no additive. The coulombic efficiencies could not be fully realised in the full cell due to inefficiencies in the nickel electrode reactions, e.g., limited capacity caused by the surface area of active material at the nickel electrode.

As expected from the results of cyclic voltammetry and linear sweep voltammetry, TEAH and TEAB show a slight decrease in the voltaic efficiency due to the effect of these additives on zinc reduction/oxidation overpotentials. Interestingly, PEG 200 produces a poorer performance compared with no additive. This is contrary to the results of the zinc half-cell tests which suggest an improvement in performance may be expected with this additive. This might be explained by the instability of the PEG 200 additive at the nickel electrode where it can be oxidised and consequently leading to deterioration in the cell performance. It is however noted that the mechanism by which PEG 200 additives impact zinc deposition and dissolution is not fully understood, and remains under investigation.

**Fig. 8a** reports the cell voltage *vs.* time response during the first five cycles of a charge/discharge cycling experiment carried out in the zinc-nickel flow cell with TEAH additive as an illustration example. During the first charge the cell voltage is almost constant at around 1.95 V but during the second charge, the cell voltage commences at a lower value, 1.85 V, and increases to 1.94 V by the end of the 15 min charge duration. This is associated with the nucleation overpotential of zinc onto the graphite substrate. The gradually reducing charging voltage over subsequent cycles are a result of the diminishing effect of nucleation and the increasing electrochemically active surface area from the deposited zinc. In all cases illustrated in **Fig 7**, the charge/discharge voltages and coulombic efficiencies stabilise after 5-10 cycles and remain relatively consistent thereafter. **Fig. 8b** demonstrates the 50 charge/discharge curve of TEAH, which is stable with no sign of decay in performance. At present, all experiments have been extended only to a small number of cycles. It is clearly essential to carry out experiments over a much longer cycle life and including a higher state of charge. It should be emphasised that the promising flow cell performance has been achieved without optimisation of either the cell design or the operating conditions. Other parameters such as the electrolyte flow rate, additives concentration, and further electrode materials also remain to be studied.

#### **4. Conclusions**

In this study, 16 additives for zinc morphology modification are tested and characterised under identical experimental conditions. From cyclic voltammetry, linear sweep voltammetry, and half-cell cycling tests on the quaternary ammonium additives, a clear trend in overpotentials of zinc deposition/dissolution reactions increasing according to the size of the quaternary ammonium group has been observed, following the order: methyls → ethyls → hexadecyl trimethyls → propyls → butyls. Clearly, shorter alkyl chains in these additives result in smaller overpotentials for zinc deposition and dissolution. The larger overpotentials

associated with longer alkyl chains in these additives result in the polarisation of zinc reduction and oxidation reactions, which in turn will attenuate the voltaic efficiency of a full cell or battery system. Based on evaluation, TEAH, TEAB and PEG 200 are identified as promising additives and tested in a zinc-nickel flow cell. The resultant cycling data shows coulombic efficiencies of up to 90 %, voltaic efficiencies of up to 88 % and energy efficiencies of up to 79 %, with TEAH and TEAB, confirming that these are the most promising additives in terms of electrochemical performance. Further work is ongoing to optimise the concentrations of these additives, and investigate their effect on the nickel electrode through cyclic voltammetry and full cell cycling. The influence of additional factors such as electrolyte flow rate, temperature and current density on zinc-nickel flow cell performance is also to be studied.

## **Acknowledgements**

The authors would like to acknowledge the support received from C-Tech Innovation Ltd (John Collins and David Hall) and WhEST Ltd (Ian Whyte). They also thank Professor Derek Pletcher of the University of Southampton for providing critical comments which greatly improved the manuscript.

Funding: This work was supported by the EPSRC Supergen Energy Storage Project (grant number: EP/P003494/1) entitled ‘Zinc-Nickel Redox Flow Battery for Energy Storage’; the EPSRC PhD studentship as a Doctoral Training Partnership (DTP); and the support from the College of Engineering, Mathematics and Physical Sciences in the University of Exeter

## References

- [1] Z.G. Yang, J.L. Zhang, M.C. W. Kintner-Meyer, X.C. Lu, D.W. Choi, J.P. Lemmon, J. Liu, Electrochemical Energy Storage for Green Grid, *Chem. Rev.* 111 (2011) 3577–3613.
- [2] M. Skyllas-Kazacos, M.H. Chakrabarti, S.A. Hajimolana, F.S. Mjalli, M. Saleem, Progress in Flow Battery Research and Development, *J. Electrochem. Soc.* 158 (2011) R55–79.
- [3] P.K. Leung, X. Li, C. Ponce de Leon, L. Berlouis, C.T.J. Low, F.C. Walsh, Progress in Redox Flow Batteries, Remaining Challenges and Their Applications in Energy Storage, *RSC Adv.* 2 (2012) 10125-10156.
- [4] P.C. Butler, P.A. Eidler, P.G. Grimes, S.E. Klassen, R.C. Miles, Zinc bromine batteries in D. Linden, T.B. Reddy (Eds.), *Handbook of Batteries*, 3<sup>rd</sup> Edition, Ch39 (2002), McGraw-Hill.
- [5] J. Pan, L. Ji, Y. Sun, P. Wan, J. Cheng, Y. Yang, M. Fan, Preliminary study of alkaline single flowing Zn-O<sub>2</sub> battery, *Electrochem. Commun.* 11 (2009) 2191-2194.
- [6] F.C. Walsh, L.F. Arenas-Martinez, L. Berlouis, C. Ponce de León, G. Nikiforidis, D. Hodgson, D. Hall, The development of Zn-Ce flow batteries for energy storage and their continuing challenges, *ChemPlusChem* 80 (2015) 288-311.
- [7] J. Winsberg, T. Janoschka, S. Morgenstern, T. Hagemann, S. Muench, G. Hauffman, J.-F. Gohy, M.D. Hager, U.S. Schubert, Poly(TEMPO)/zinc hybrid-flow battery: A novel, “green,” high voltage, and safe energy storage system, *Adv. Mater.* 28 (2016) 2238-2243.
- [8] A. Khor, P. Leung, M.R. Mohamed, C. Flox, Q. Xu, L. An, R.G.A. Wills, J.R. Morante, A.A. Shah, Review of zinc based hybrid flow batteries: From fundamentals to applications, *Material Today Energy* 8 (2018) 80-108.
- [9] D. Coates, A. Charkey, Nickel-zinc batteries in D. Linden, T.B. Reddy (Ed.), *Handbook of Batteries*, 3<sup>rd</sup> Edition, McGraw-Hill Ch31 (2002) 1-37.
- [10] X. Li, D. Pletcher, C. Ponce-de-León, F.C. Walsh, R.G.A. Wills, Zinc-based flow batteries for medium- and large-scale energy storage in C. Menictas, M. Skyllas-Kazacos, T.M. Lim (Ed.), *Advances in batteries for large- and medium-scale energy*

- storage: Applications in power systems and electric vehicles, Woodhead Publishing. Ch9 (2015) 293-315.
- [11] P.K. Leung, C. Ponce-de-Leon, C.T.J. Low, F.C. Walsh, Zinc deposition and dissolution in methanesulfonic acid onto a carbon composite electrode as the negative electrode reactions in a hybrid redox flow battery, *Electrochim. Acta* 56 (2011) 6536-6546.
- [12] K. Bass, P.J. Mitchell, G.D. Wilcox, Methods for the reduction of shape change and dendritic growth in zinc-based secondary cells, *J. Power Sources* 35 (1991) 333-351.
- [13] J. McBreen, E. Gannon, The electrochemistry of metal oxide additives in pasted zinc electrodes, *Electrochim. Acta* 26 (1981) 1439-1446.
- [14] Y. Wen, J. Cheng, L. Zhang, X. Yan, Y. Yang, The inhibition of the spongy electrocrystallisation of zinc from doped flowing alkaline zincate solutions, *J. Power Sources* 193 (2009) 890-894.
- [15] I. N. Justinijanovic, J. N. Jovicevic, A. R. Despic, the effect of foreign atoms on the properties of electrolytic zinc powders, *J. Applied Electrochemistry* 3 (1973) 193-200.
- [16] Y.F. Yuan, J.P. Tu, H.M. Wu, S.F. Wang, W.K. Zhang, H. Huang, Effects of stannous ions on the electrochemical performance of the alkaline zinc electrode, *J. Applied Electrochemistry* 37 (2007) 249-253.
- [17] H.I. Kim, H.C. Kim, SnO additive for dendritic growth suppression of electrolytic zinc, *Journal of Alloys and Compounds* 645 (2015) 7-10.
- [18] J. McBreen, E. Gannon, Bismuth oxide as an additive in pasted zinc electrodes, *J. Power Sources* 159 (1985) 169-177.
- [19] B.S. Kwak, D.Y. Kim, S.S. Park, B.S. Kim, M. Kang, Implementation of stable electrochemical performance using a  $\text{Fe}_{0.01}\text{ZnO}$  anodic material in alkaline Ni-Zn redox battery, *Chemical Engineering Journal*. 281 (2015) 368-378.
- [20] J.M. Wang, L. Zhang, C. Zhang, J. Q. Zhang, Effects of bismuth ion and tetrabutylammonium bromide on the dendritic growth of zinc in alkaline zincate solutions, *J. Power Sources*. 102 (2001) 139-143.
- [21] R.F. Thornton, E.J. Carlson, Properties of alternate electrolytes for secondary zinc batteries, *J. Electrochem. Soc.* 127 (1980) 1448-1452.

- [22] R. Winand, Electrodeposition of Zinc and Zinc Alloys, in *Modern Electroplating*, 4<sup>th</sup> Edition, M. Schlesinger, M. Paunovic (Eds.), Electrochemical Society, 2000.
- [23] J.W. Diggle, A. Damjanovic, The inhibition of dendritic electrocrystallization of zinc from doped alkaline zincate solutions, *J. Electrochem. Soc.* 119 (1972) 1649-1658.
- [24] J. Zhu, Y. Zhou, C. Gao, Influence of surfactants on electrochemical behaviour of zinc electrodes in alkaline solution, *J. Power Sources* 72 (1998) 231-235.
- [25] G.D. Wilcox, P.J. Mitchell, Electrolyte additives for zinc-anoded secondary cells II. Quaternary ammonium compounds, *J. Power Sources* 32 (1990) 31-41.
- [26] C.J. Lan, C.Y. Lee, T.S. Chin, Tetra-alkyl ammonium hydroxides as inhibitors of Zn dendrite in Zn-based secondary batteries, *Electrochim. Acta* 52 (2007) 5407–5416.
- [27] Y. Wen, T. Wang, J. Cheng, J. Pan, G. Cao, Y. Yang, Lead ion and tetrabutylammonium bromide as inhibitors to the growth of spongy zinc in a single flow zinc/nickel batteries, *Electrochim. Acta* 59 (2012) 64-68.
- [28] J.L. Ortiz-Aparicio, Y. Meas, G. Trejo, R. Ortega, T.W. Chapman, E. Chainet, Effects of organic additives on zinc electrodeposition from alkaline electrolytes, *J. Appl. Electrochem.* 43 (2013) 289–300.
- [29] E. Frackowiak, M. Kiciak, The influence of polyethylene glycol on some properties of zinc electrodes, *Electrochim. Acta* 29 (1984) 1359-1363.
- [30] J.C. Ballesteros, P. Diaz-Arista, Y. Meas, R. Ortega, G. Trejo, Zinc electrodeposition in the presence of polyethylene glycol 20000, *Electrochim. Acta* 52 (2007) 3686–3696.
- [31] S.J. Banik, R. Akolkar, Suppressing dendrite growth during zinc electrodeposition by PEG-200 Additive, *J. Electrochem. Soc.* 160 (2013) D519–D523. doi:10.1149/2.040311jes.
- [32] S.J. Banik, R. Akolkar, Suppressing dendritic growth during alkaline zinc electrodeposition using polyethylenimine additive, *Electrochim. Acta* 179 (2015) 475-481.
- [33] A. Nakata, H. Arai, T. Yamane, T. Hirai, Z. Ogumi, Preserving Zinc Electrode Morphology in Aqueous Alkaline Electrolytes Mixed with Highly Concentrated Organic Solvent, *J. Electrochem. Soc.* 163 (2016) A50-A56.

- [34] J.O'M. Bockris, Z. Nagy, A. Damjanovic, On the Deposition and Dissolution of Zinc in Alkaline Solutions, *J. Electrochem. Soc.* (1972) 285-295.

**Table 1.** Additives under investigation

Additive	Concentration (mmol dm <sup>-3</sup> )	Details	Chemical Structure
Bismuth (III) Oxide (Bi <sub>2</sub> O <sub>3</sub> )	1	Alfa Aesar, 99.975 %	
Tin (II) Chloride (SnCl <sub>2</sub> )	1	Sigma-Aldrich, 98 %	
Tin (II) Oxide (SnO)	1	Sigma-Aldrich, 99.99 %	Sn=O
Iron (II) Bromide (FeBr <sub>2</sub> )	1	Sigma-Aldrich, 98 %	Br—Fe—Br
Polyethylenimine (PEI 800)	5	Sigma-Aldrich, M.W. = 800 g mol <sup>-1</sup>	
Polyethylene glycol (PEG 200)	5	Sigma-Aldrich, M.W. = 200 g mol <sup>-1</sup>	
Tetramethylammonium hydroxide (TMAH)	5	Alfa Aesar, 25 % wt. in H <sub>2</sub> O	
Tetraethylammonium hydroxide (TEAH)	5	Sigma-Aldrich, 20 % wt. in H <sub>2</sub> O	
Tetrapropylammonium hydroxide (TPAH)	5	Alfa Aesar, 1 M solution	
Tetrabutylammonium hydroxide (TBAH)	5	Sigma-Aldrich, 40 % wt. in H <sub>2</sub> O	
Hexadecyltrimethylammonium hydroxide (HDTMAH)	5	Tokyo Chemical Industry, 10 % wt. in H <sub>2</sub> O	
Tetramethylammonium bromide (TMAB)	5	Sigma-Aldrich, 98 %	
Tetraethylammonium bromide (TEAB)	5	Sigma-Aldrich, reagent grade, 98 %	
Tetrapropylammonium bromide (TPAB)	5	Alfa Aesar, 98 %	
Tetrabutylammonium bromide (TBAB)	5	Sigma-Aldrich, 98 %	
Cetrimonium bromide (CTAB)	5	Alfa Aesar, 98 %	

**Table 2.** Results of cyclic voltammetry, linear sweep voltammetry and zinc half-cell cycling. Charge ratios and peak separation taken from Fig. 2. Cathodic and anodic current densities taken from Fig. 3. Half-cell coulombic efficiencies averaged over 11 cycles in a stirred 6 M KOH + 0.5 M ZnO electrolyte solution containing additives. Zinc deposited on a graphite/polyvinylidene fluoride electrode at  $-100 \text{ mA cm}^{-2}$  for 12 min and dissolved at a current density of  $100 \text{ mA cm}^{-2}$  to a cut-off potential of 0.8 V vs. Hg/HgO. Temperature: 293 k.

<b>Additive</b>	<b>Anodic/cathodic charge ratio, <math>Q_{\text{anodic}}/Q_{\text{cathodic}}</math></b>	<b>Anodic/cathodic peak separation, <math>\Delta E_p</math> (mV)</b>	<b>Cathodic current density <math>\text{j/mAcm}^{-2}</math> (<math>\eta = -50\text{mV}</math>)</b>	<b>Anodic current density, <math>\text{j/mAcm}^{-2}</math> (<math>\eta = 50\text{mV}</math>)</b>	<b>Half-cell coulombic efficiency (%)</b>
No Additive	0.76	220	34	78	87
Bi <sub>2</sub> O <sub>3</sub>	0.82	227	30	67	92
SnCl <sub>2</sub>	0.80	218	37	70	84
SnO	0.78	222	35	74	88
FeBr <sub>2</sub>	0.79	239	34	74	88
PEI 800	0.83	384	5	7	94
PEG 200	0.85	219	28	75	95
TMAB	0.83	231	32	77	88
TEAB	0.85	212	32	79	95
TPAB	0.91	305	9	12	97
TBAB	0.93	553	4	6	74
CTAB	0.90	271	13	44	97
TMAH	0.82	230	32	79	89
TEAH	0.88	207	31	78	97
TPAH	0.95	309	8	11	94
TBAH	0.93	548	4	6	32
HDTMAH	0.87	268	15	41	93

**Table 3.** Coulombic, voltaic, and energy efficiencies for a zinc-nickel flow cell during 50 charge/discharge cycles in a 6 M KOH + 0.5 M ZnO solution with no additive and 5 mM PEG 200, TEAH and TEAB. Charged at 20 mA cm<sup>-2</sup> for 15 min and discharged at 20 mA cm<sup>-2</sup> to a cut off potential of 0.8 V. Graphite/polyvinylidene fluoride negative electrode substrate, sintered nickel positive electrode with an inter-electrode gap of 1.2 cm. Electrode area: 1 cm<sup>2</sup>. Electrolyte flow rate: 9.7 cm s<sup>-1</sup>. Temperature: 293 K.

<b>Additive</b>	<b>Coulombic Efficiency (%)</b>	<b>Voltaic Efficiency (%)</b>	<b>Energy Efficiency (%)</b>
No Additive	77	90	69
PEG 200	74	86	64
TEAH	90	88	79
TEAB	89	88	77

## Figure Captions

**Fig. 1.** Cyclic voltammogram recorded at a graphite/polyvinylidene fluoride electrode (area  $0.25 \text{ cm}^2$ ) in an electrolyte solution containing  $4 \text{ M NaOH} + 0.1 \text{ M ZnO}$ . Potential sweep rate:  $10 \text{ mV s}^{-1}$ . Temperature:  $293 \text{ K}$ .

**Fig. 2.** Cyclic voltammograms recorded at a polished graphite/polyvinylidene fluoride electrode (area  $0.25 \text{ cm}^2$ ) in electrolyte solutions containing  $6 \text{ M KOH} + 0.5 \text{ M ZnO} +$  various additives: (a) metallic additives, (b) non-ionic surfactants, (c) quaternary ammonium bromides, (d) quaternary ammonium hydroxides. Potential sweep rate:  $20 \text{ mV s}^{-1}$ . Temperature:  $293 \text{ K}$ .

**Fig. 3.** SEM images of zinc deposits from electrolyte solutions containing  $6 \text{ M KOH} + 0.5 \text{ M ZnO} + 1 \text{ mM}$  metallic additives or  $5 \text{ mM}$  non-ionic surfactants: (a) no additive, (b)  $\text{Bi}_2\text{O}_3$ , (c)  $\text{SnCl}_2$ , (d)  $\text{SnO}$ , (e)  $\text{FeBr}_2$ . (f) PEI 800, (g) PEG 200. Each deposit was obtained on a polished graphite/polyvinylidene fluoride electrode substrate (area  $0.25 \text{ cm}^2$ ) at a current density of  $20 \text{ mA cm}^{-2}$  for 1 h. SEM magnifications: 500 (inserts: 10 k).

**Fig. 4.** SEM images of zinc deposits from electrolyte solutions containing  $6 \text{ M KOH} + 0.5 \text{ M ZnO} + 5 \text{ mM}$  various quaternary ammonium bromide additives: (a) TMAB, (b) TEAB, (c) TPAB, (d) TBAB, (e) CTAB. Each deposit was obtained at a polished graphite/polyvinylidene fluoride electrode substrate (area  $0.25 \text{ cm}^2$ ) at a current density of  $20 \text{ mA cm}^{-2}$  for 1 h. SEM magnifications: 500 (inserts: 10 k).

**Fig. 5.** SEM images of zinc deposits from electrolyte solutions containing  $6 \text{ M KOH} + 0.5 \text{ M ZnO} + 5 \text{ mM}$  various quaternary ammonium hydroxide additives: (a) TMAH, (b) TEAH, (c) TPAH, (d) TBAH, (e) HDTMAH. Each deposit was obtained at a polished graphite/polyvinylidene fluoride electrode substrate (area  $0.25 \text{ cm}^2$ ) at a current density of  $20 \text{ mA cm}^{-2}$  for 1 h. SEM magnifications: 500 (inserts: 10 k).

**Fig. 6.** Potential vs. time plots during the deposition and dissolution cycling of zinc in a stirred electrolyte solution of 6 M KOH + 0.5 M ZnO without and with additive of 5 mM TEAH. During each cycle, the zinc was deposited on a graphite/polyvinylidene fluoride electrode at a cathodic current density of  $-100 \text{ mA cm}^{-2}$  for 12 min and dissolved at an anodic current density of  $+100 \text{ mA cm}^{-2}$  to a cut off potential of  $-1.0 \text{ V vs. Hg/HgO}$ . Temperature: 293 K.

**Fig. 7.** Energy efficiencies as a function of cycle number for a zinc-nickel flow cell during the 50 charge/discharge cycles in an electrolyte solution of 6 M KOH + 0.5 M ZnO with no additive ( $\bullet$ ) and with 5 mM additive of PEG200 ( $\blacksquare$ ), TEAB ( $\blacklozenge$ ), and TEAH ( $\blacktriangle$ ). Cell charged at  $20 \text{ mA cm}^{-2}$  for 15 min and discharged at the same current density until the voltage dropped to 0.8 V. Graphite/polyvinylidene fluoride negative electrode, sintered nickel positive electrode, inter-electrode gap of 1.2 cm. Electrode area:  $1 \text{ cm}^2$ . Electrolyte flow rate:  $9.7 \text{ cm s}^{-1}$ . Temperature: 293 K.

**Fig. 8.** Cell voltage vs. time responses for (a) the initial 5 charge/discharge cycles and (b) the 50 charge/discharge cycles of a zinc-nickel flow cell. Cell charged at  $20 \text{ mA cm}^{-2}$  for 15 min and discharged at the same current density to a cut-off potential of 0.8 V. Graphite/polyvinylidene fluoride negative electrode, sintered nickel positive electrode, inter-electrode gap 1.2 cm. 6 M KOH + 0.5 M ZnO + 5 mM TEAH electrolyte solution. Electrode area:  $1 \text{ cm}^2$ . Electrolyte flow rate:  $9.7 \text{ cm s}^{-1}$ . Temperature: 293 K.

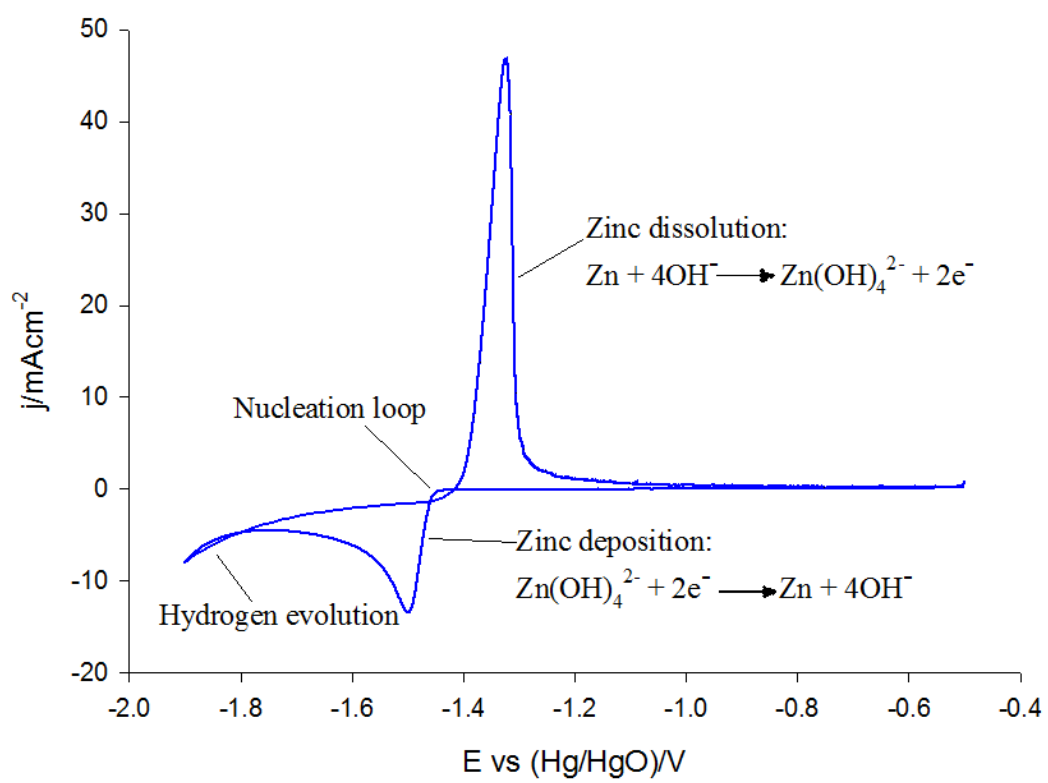


**Fig. 1**

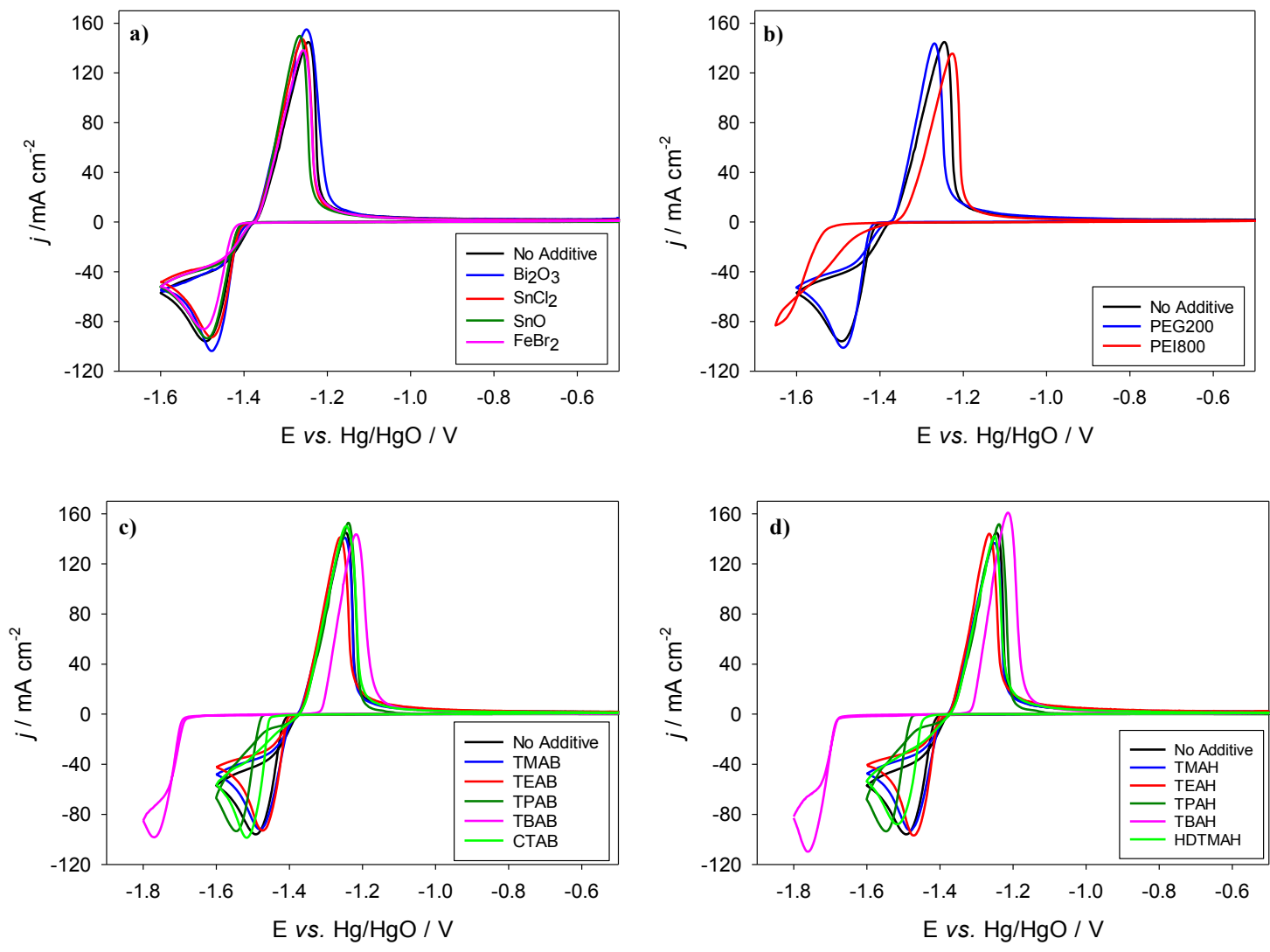


**Fig. 2**

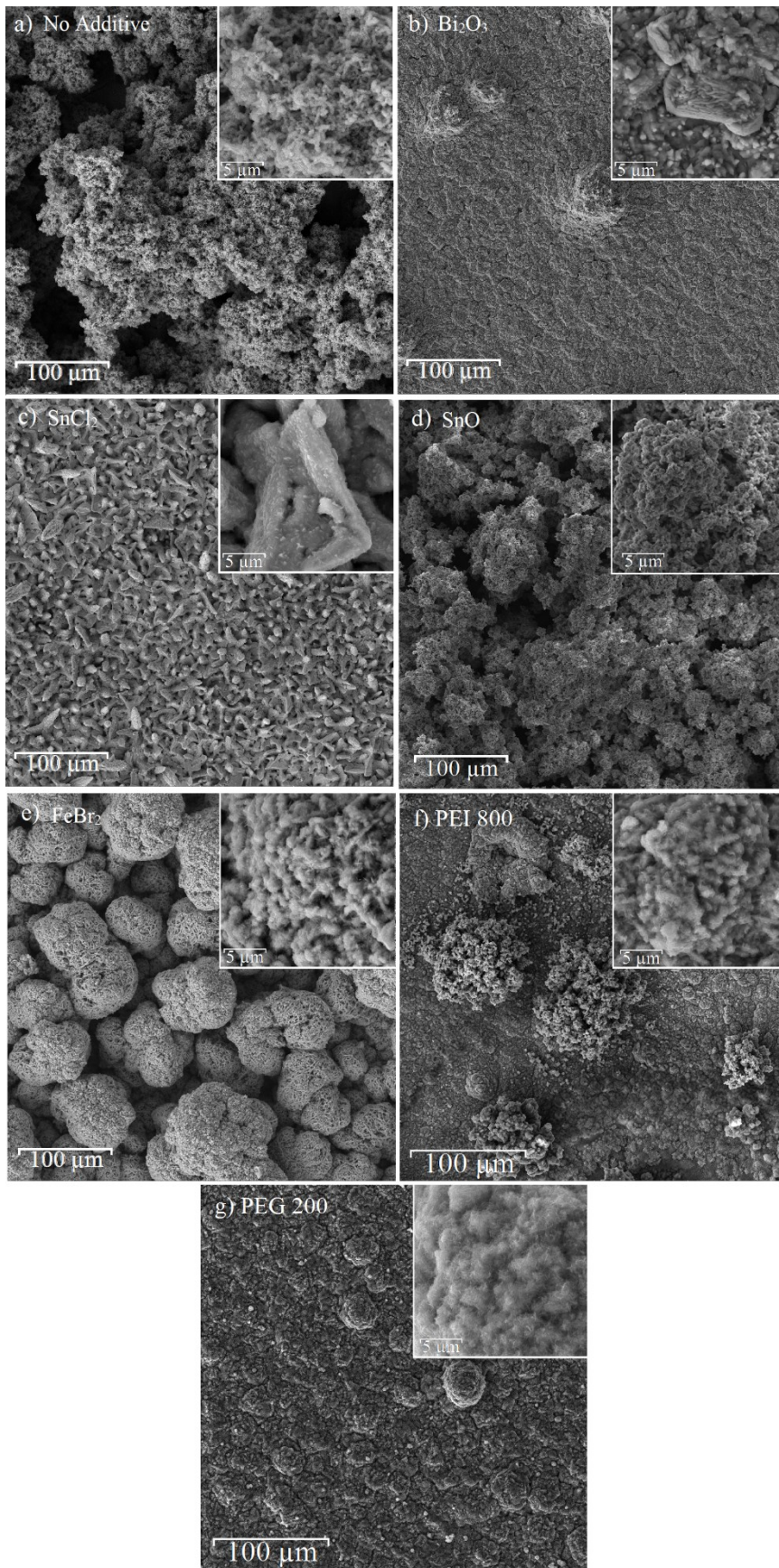


**Fig. 3**

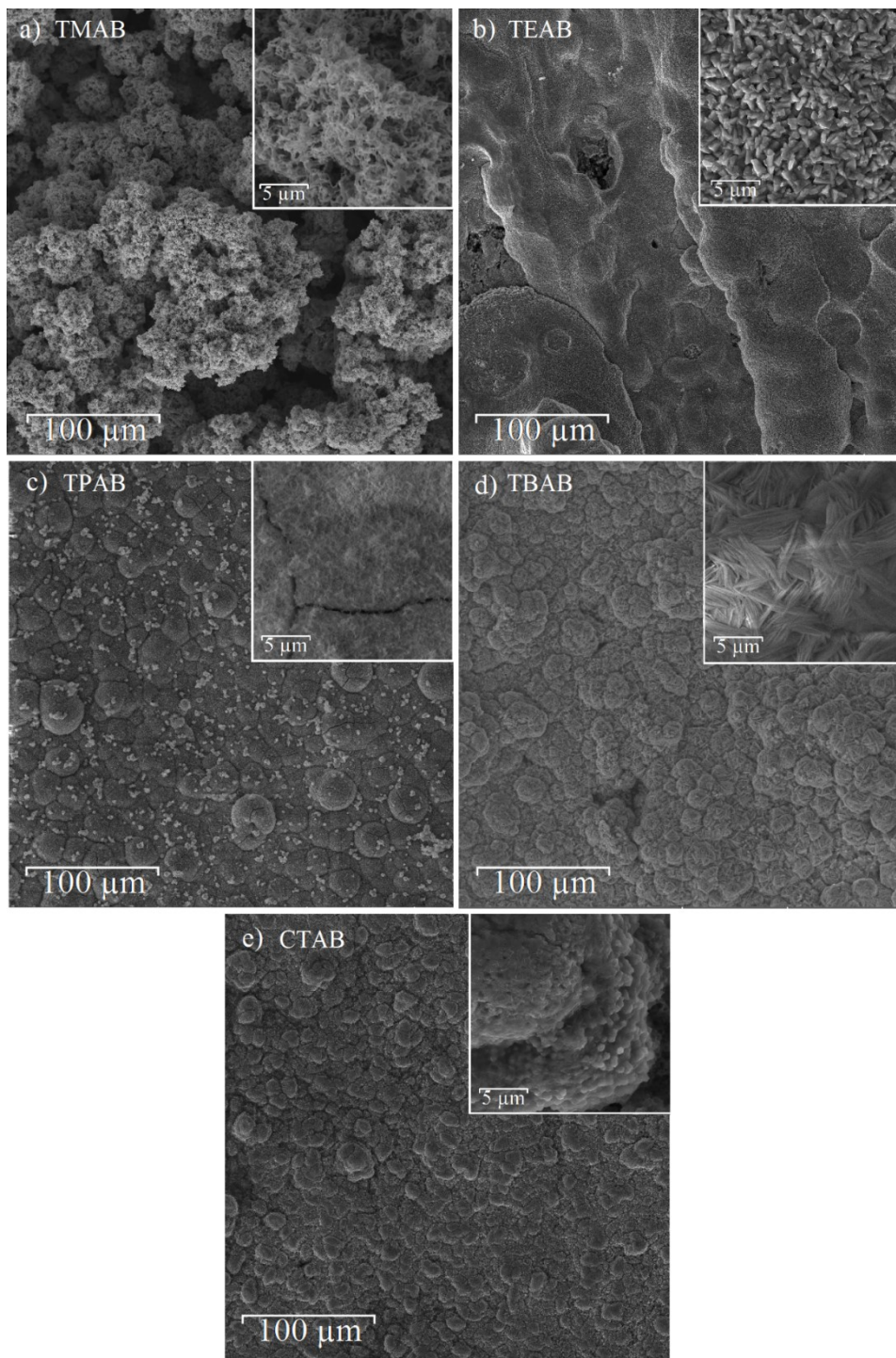


**Fig. 4**

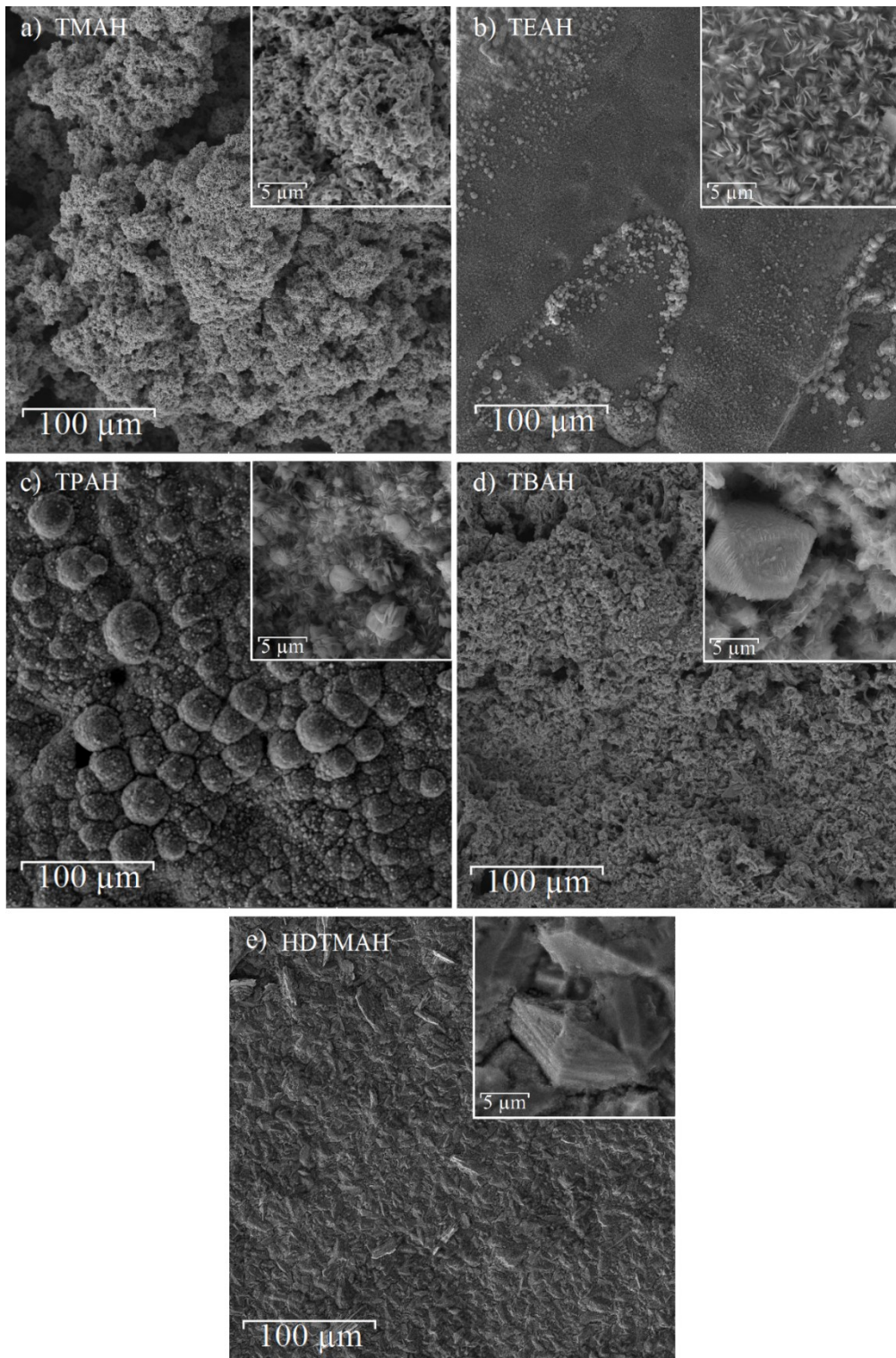


**Fig. 5**

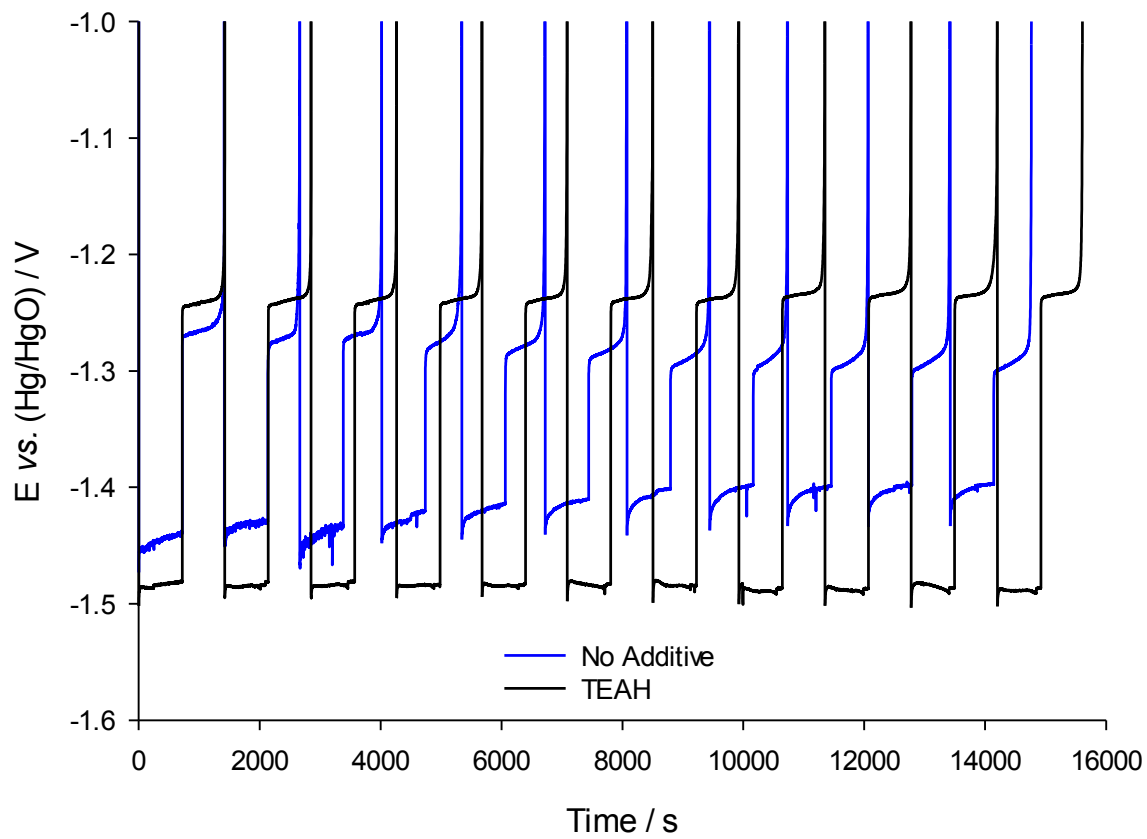


**Fig. 6**

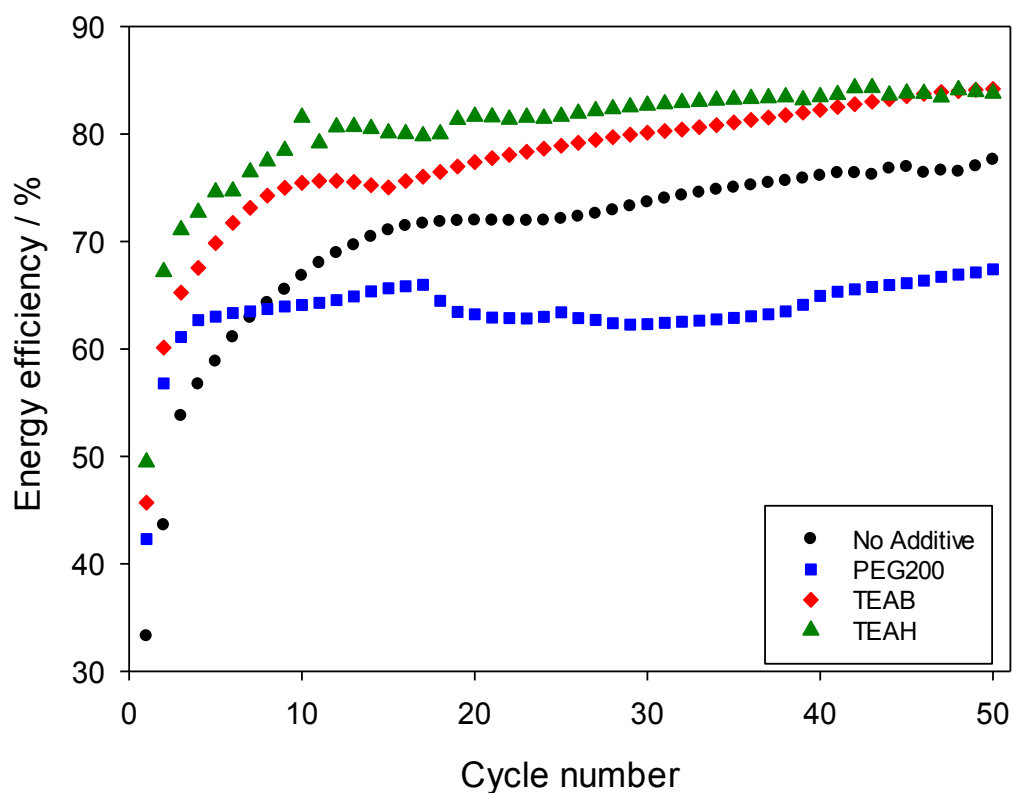
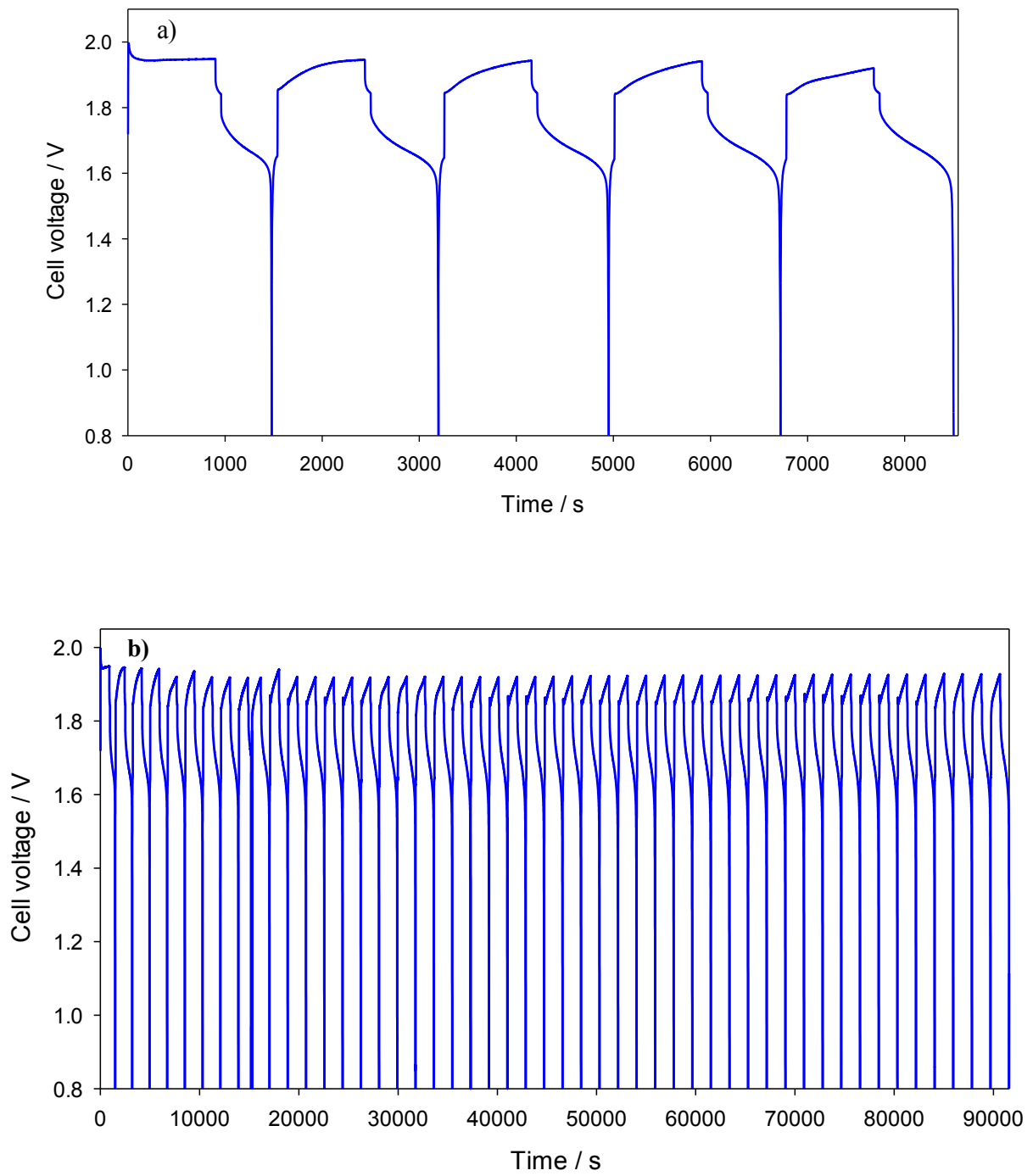


Fig. 7



**Fig. 8**